N92-22722

FIBER-OPTIC PUSH-PULL SENSOR SYSTEMS

David L. Gardner, David A. Brown, and Steven L. Garrett
Code PH/Gd, Department of Physics
Naval Postgraduate School
Monterey, CA 93943

ABSTRACT

Fiber-optic push-pull sensors are those which exploit the intrinsically differential nature of an interferometer with concommitant benefits in common-mode rejection of undesired effects. Several fiber-optic accelerometer and hydrophone designs are described. Additionally, the recent development at the Naval Postgraduate School of a passive low-cost interferometric signal demodulator permits the development of economical fiber-optic sensor systems.

INTRODUCTION

Optical fiber sensors have been represented as being of rather remarkable sensitivity, even to the point of violating the Second Law of Thermodynamics [1], [2], [3], and easy to fabricate. Obviously, optical fiber sensor designs have not always realized these early expectations in sensitivity [4] and geometric flexibility. However, sensors using technology developed for the communications industry do offer the possibility of remote sensing, with no electrical power required for signal amplification, at distances of 20 km or more. Further, fiber sensors, and the compatible communication lines to them, offer several advantages, among which are the immunity from electromagnetic interference, light weight, low power requirements, low crosstalk, and reduced risk of shock or spark hazards [3]. All the sensors described in this paper exploit developments in communications technology; accordingly, each can be used to detect stimuli kilometers away from the transmitting light source and receiving electronics.

We divide optical fiber sensors into two general categories: intrinsic and extrinsic. Extrinsic fiber sensors are those in which the light, at some point in the sensing operation, leaves the fiber. An example is the Fabry-Perot interferometer, in which the light leaves the fiber and impinges on some sensing mechanism from which it is reflected. The reflected light is then combined interferometrically with the incident light, and the resulting optical fringe pattern is representative of the stimuli. Intrinsic fiber sensors are those in which the light never leaves the fiber; this type of sensor facilitates the relatively easy construction of push-pull optical fiber sensors.

In push-pull optical fiber sensors, an optical fiber coupler bifurcates the light power within a single fiber into two fibers forming the two legs of the interferometer. The two legs can then be made to operate in a differential mode, or push-pull, in contrast to sensors in which the sensor response to a stimuli is compared to an isolated reference leg. Since optical fibers are neither intrinsically sensitive or selective to stimuli [5], considerable difficulty exists in attempting to create an isolated reference insensitive to all environmental stimuli. Placing the two legs of a push-pull sensor in close proximity exploits the common-mode rejection intrinsic to an interferometric sensor, thus minimizing the effects of unwanted environmental effects. The sensor design effort can then focus on enhancing the stimuli of interest, and achieve greater sensitivity since both legs of the interferometer are responsive.

Interferometric fiber-optic sensors generate signals proportional to the phase differences between the light waves propagating in the two interferometer legs [6]. Since the signals are phase differences, the sensor is not hostage to fluctuations in the transmitted light power, a problem common to sensors whose output light intensity is proportional to the stimuli intensity.

Phase shift in an optical fiber can be caused by several mechanisms, such as variation in fiber length, polarization, index of refraction within the core, or variations in the core diameter. The optical phase shift, $\delta\phi$, is given in general form by [7]:

$$\delta\phi = \beta\Delta L + L\Delta\beta = \beta\Delta L + L\left(k\Delta n + \frac{\partial\beta}{\partial a}\Delta a\right) \qquad (1)$$

Here, β is the optical propagation constant along the fiber axis ($\beta=2\pi/\lambda$, where λ is the optical wavelength in the fiber core), L is the fiber length responsive to the stimuli inducing the phase shift, k is the optical wave number in vacuum, n is the index of refraction of the fiber core, and a is the fiber core diameter, typically 5-8 mm in the single-

mode fiber used for the sensors reported herein. Changes in any of the parameters in eq. (1) will induce a phase shift; for the sensors to be described, the length of the fiber is modulated by the stimuli of interest.

FIBER-OPTIC ACCELEROMETERS

Two designs for fiber-optic interferometric accelerometers have been developed at the Naval Postgraduate School (NPS). The first (Fig. 1) consists of a seismic mass supported by two mandrels around which are wrapped the two legs of the interferometer [8], [9]. The mandrels are constructed from castable soft rubber, having a Poisson's ratio of nearly one-half, and act as transformers of longitudinal compression into circumferential strain. When the accelerometer case is displaced, the seismic mass compresses one of the mandrels while relieving the other. Accordingly, the two fibers wrapped around the mandrels experience strains of opposite sign, a feature of push-pull sensor design. The fibers reject changes in ambient temperature and pressure by exploiting the common-mode rejection which is also a feature of push-pull sensors. The acceleration sensitivity of a sensor of this type, using a 640 gm seismic mass and eight meters of fiber in each leg, is 10,000 radians/g [10].

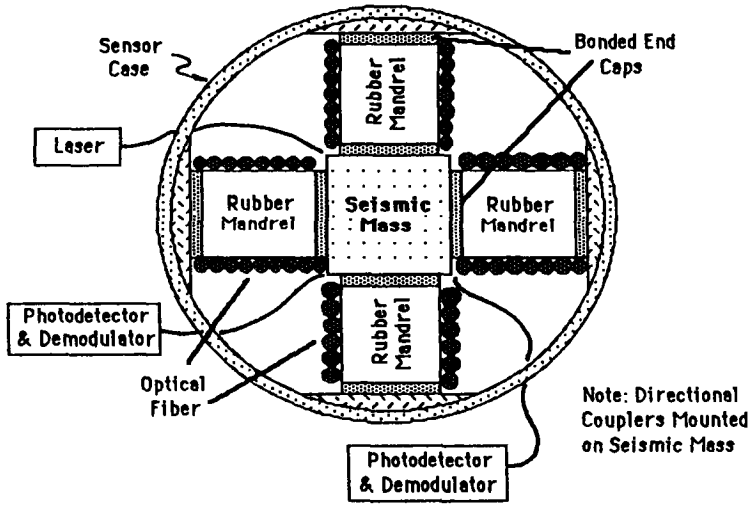

Figure 1. Sketch of a push-pull accelerometer using optical fiber wrapped rubber mandrels supporting a seismic mass. When the sensor case is displaced in a direction along the axis of a supporting mandrel pair, one of the mandrels is compressed while the other is relieved; accordingly, the optical fiber around one mandrel is stretched while the other is relieved.

Figure 2 is a plot of the interferometric signal output from this type of sensor compared to that of a high-sensitivity accelerometer. Novel techniques recently developed at NPS for demodulating the interferometric signals will be presented later in this paper.

Three such fiber-optic accelerometers placed on orthogonal axes and sharing a common seismic mass constitute a three-axis accelerometer. In all cases, the fiber-optic couplers used must remain within the accelerometer housing so as to not jeopardize the common-mode rejection of undesired environmental effects.

The second accelerometer design is sketched in Figure 3 [11], [12]. When the sensor is accelerated, strains are induced in the two thin circular plates. The disks are attached at the centers with the siesmic mass, which can be adjusted to achieve a desired resonance frequency. The two optical fiber legs forming the interferometer are wound in concentric, pancake-like coils, and are epoxied to each of the inside surfaces of the plates. When the sensor is displaced, the surfaces experience strains, of opposite sign, which are detected by the bonded fiber coils. As with the previous design, the two coils experience similar responses to unwanted influences of temperature and pressure by utilizing the common-mode rejection intrinsic to the interferometer. The acceleration sensitivity of a sensor of this type, using a 34 gm seismic mass and five meters of fiber in each leg, is 49 radians/g.

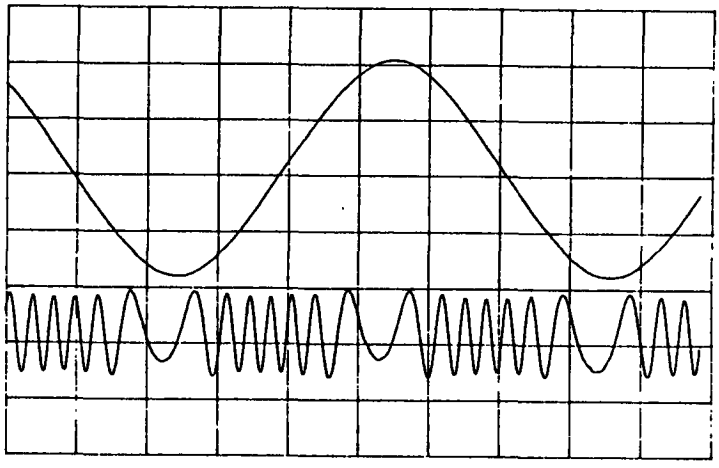

Figure 2. Sketch of an oscilloscope display of the output signal from a push-pull optical fiber sensor. The upper trace is from a conventional accelerometer and the lower trace is from an interferometric push-pull sensor.

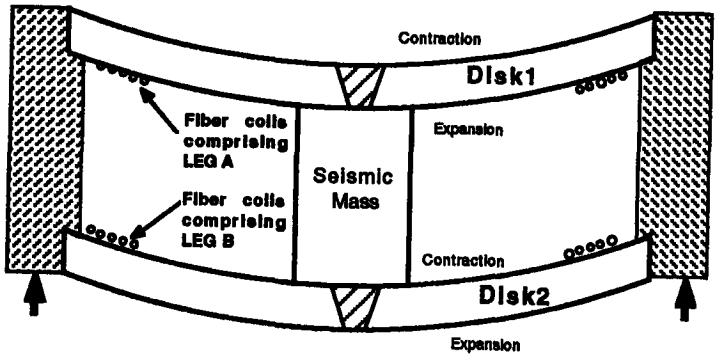

Figure 3. Sketch of a fiber-optic flexural disk accelerometer. When the case is accelerated, the inner surfaces of the two disks experience strains of oppossite sign. The optical fiber coils bonded to the surfaces also experience strains of opposite sign.

FIBER-OPTIC HYDROPHONES

Directional Hydrophones

If the above designs are placed within a neutrally-buoyant container and then placed in water [13], [14], the container will experience acoustically induced accelerations according to the linearized Euler equation:

$$\frac{\partial v}{\partial t} = -\frac{1}{\rho}\nabla P, \tag{2}$$

where ρ is the fluid density. Accordingly, the sensor becomes bi-directional. The first sensor design is insensitive to changes in temperature or hydrostatic pressure (which deforms the neutrally buoyant case) since these effects cause identical changes in the two mandrels and are rejected by the differential behavior of the interferometer. The second design is insensitive since hydrostatic pressure causes both plates to experience similar strain.

Omni-directional Flexural Plate Hydrophone

The pressure-induced strain experienced by the two circular plates afforded the opportunity to construct an omni-directional sensor by placing the coils so as to enhance this response [15], [16], [17]. A sensor so constructed will be insensitive to acceleration, and the sensitivity can be increased by placing coils appropriately on both sides of the plates (Fig. 4). We have constructed and tested several of these "flexural plate" hydrophones. The theoretical sensitivity based upon the elastic properties of the plate materials and boundary conditions is in excellent agreement with the measured sensitivity for both acoustic and hydrostatic pressure in water and air.

We have also constructed four-coil versions of this dual-plate hydrophone made entirely from a high tensile strength castable elastomer having a low dynamic Young's modulus with a temperature coefficient of 0.3%/°C within the range of oceanic temperatures [18]. The four coils and coupler are cast into the unit and the gap between the plates is chosen so that the plates touch at the maximum operating depth. This permits the maximum sensitivity consistent with the breaking strain of the optical fibers since the hydrophone does not rely on the tensile strength of the plate material alone to support the hydrophone at crush depth.

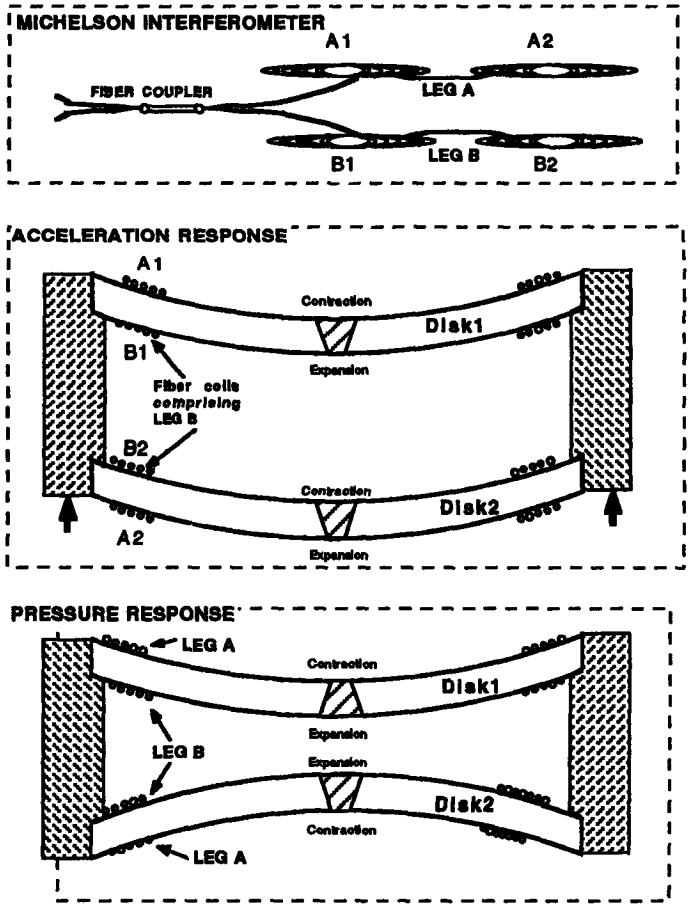

Figure 4. Sketch of a omni-directional flexural disk hydrophone interferometer and responses. The upper figure is a schematic representation of the optical fiber coupler and coils forming the Michelson interferometer. The middle figure illustrates the response of the hydrophone under acceleration; the two coils of either Leg A or Lag B experience no net change in length since one coil is stretched while the second is relieved. The lower figure illustrates the pressure response of the sensor; the strains experienced by both coils of Leg A and Leg B are of opposite sign.

Ellipsoidal Flextensional Hydrophone

When an oblate spheroidal shell, shown in Figure 5, having an aspect ratio $a/b > (2-\nu)^{1/2}$, where ν is Poisson's ratio, is subject to hydrostatic compression, the semi-major (a) axis and semi-minor axis (b) experience strains of opposite sign. If two optical fibers, which comprise the arms of an interferometer, are wound around the the semi-major axis and semi-minor axis circumferences of the oblate spheroid, pressure changes will induce a differential optical phase shift [19], [20].

As in the case of the flexural plate design, we have developed a "closed form" analytical description of this hydrophone which provides the necessary design parameters (a, b, and t) based on the choice of shell material, operating bandwidth, and maximum operating depth [21]. This design has the advantage of requiring no internal parts so that the shells can be fabricated by inexpensive methods (e.g. injection molded) after which the optical fibers can be attached to the exterior.

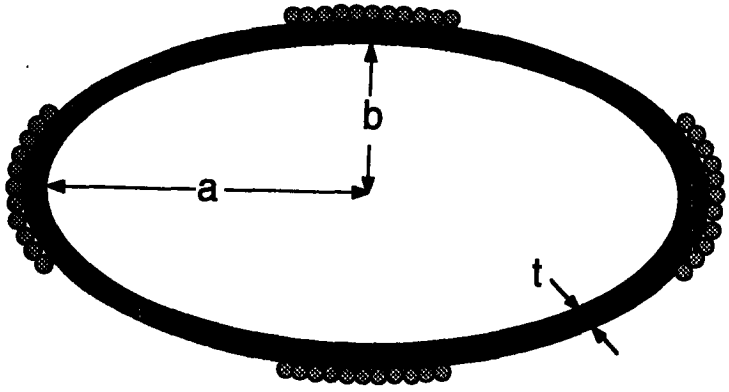

Figure 5. Cross-sectional sketch of a fiber-optic oblate spheroidal flextensional hydrophone showing the shell thickness, t, and the semi-major (a) axis and semi-minor axis (b) coil pairs. The three-dimensional shell is generated by rotation about the semi-minor axis (b).

This geometry also provides considerable flexibility in array design [22]. The hydrophone element or array to be "shaded" by varying the number of turns taken around each shell. Optical redundancy of the array to improve reliability can be accomplished by wrapping optical fiber of independent interferometers around the same shells. A pressure gradient hydrophone could be constructed by wrapping the fiber from one leg of the interferometer around the equator of one shell and the meridian of the other, and the opposite wiring for the other shell. A cardiod beam pattern could then be obtained by wrapping one leg of a second interferometer around the equators of both oblate spheroids and the other leg around the meridians so that the same two shells would give both the omni-directional and the bi-directional information. Clearly, higher-order arrays could be constructed in the same way.

Demodulation of Fiber-Optic Interferometric Signals

The most prevalent demodulation technique for 2x2 coupler-based interferometric fiber optic signals uses a laser modulated at a carrier frequency, while the phase shifts induced by the stimulus appear as side-bands [23], [24]. The modulation of the laser is accomplished by modulating the laser drive current, an approach introducing several problems among which are: 1) the requirement for laser diodes with long coherence lengths; 2) mode-hopping induced by the superimposed current modulation; 3) high setup complexity requiring FFT calibration of phase generated carrier spectral components to insure Bessel function balance and orthogonality; 4) the necessity of an optical path difference which increases susceptibility to additional laser phase noise and extraneous environmental effects; 5) fluctuations in sensor output due to scale factor instability, (scale factor quantifies the circuit's conversion of optical phase in radians to electrical output in volts), and 6) the signal induced by the stimulus appears as side-

bands of both the carrier frequency and at its harmonics; since not all harmonics are included, the total optical signal power is not available to correct for fluctuations in fringe visibility.

An ideal, equal split ratio, 3x3 coupler, has outputs with a relative phase difference of 120° [25]. This allows the generation of in-phase and quadrature signals without the real-time carrier waveform. Previous demodulator implementations using a 3x3 coupler used only two of the three available coupler outputs to produce the in-phase and quadrature signals, and these signals were again processed by the sine-cosine algorithm used for the phase generated carrier technique [26], [27]. Although this approach does alleviate many of the problems associated with phase generated carrier demodulation, the unavailability of stable 3x3 couplers postponed the practical implementation of this strategy. Recently, however, 3x3 couplers with good environmental stability and polarization insensitivity have become available [28].

In this demodulator implementation, all three outputs of the 3x3 coupler are used in a symmetric manner to re-create the phase modulating signal, $\phi(t)$ [25], [29]. No modulation of the laser wavelength is required, thereby reducing cost and complexity, and noise (there is less probability that the laser will "mode-hop"), while removing the previously described problems associated with laser modulation. The symmetric demodulation technique is capable not only of demodulating milliradian signals, it can also demodulate signals at the kiloradian levels, as opposed to the fractional radian upper limit of phase generated carrier techniques. Accordingly, the previously described push-pull sensors, which produce signals 20 to 50 dB greater than earlier sensors, can now be readily exploited. Further, this demodulator uses a simple feedback control circuit that is capable of maintaining a stable scale factor (volts/radian) in the presence of variations in both the total optical power and in the fringe visibility.

A Mach-Zehnder fiber optic interferometer consisting of a 2x2 coupler at the input and a 3x3 coupler at the output was fabricated in order to test the symmetric demodulation algorithm [Fig. 6]. The two legs of the interferometer were wrapped around separate piezoelectric cylinders which were driven 180° out-of-phase to produce large modulation amplitudes in the interferometer. The demodulator was implemented using low-cost electronic components such as AD712 and OP111 operational amplifiers, AD534 multipliers, and a DIV100 divider.

Typical phase generated carrier demodulation techniques have a one-to-one correspondence in the change in AC power and scale factor. This is very important, since, in principle, there is no way to distinguish fluctuations in scale factor from real signals. In this demodulator implementation, the scale factor is stable to better than ±5% even in the presence of optical power variations greater than 170%.

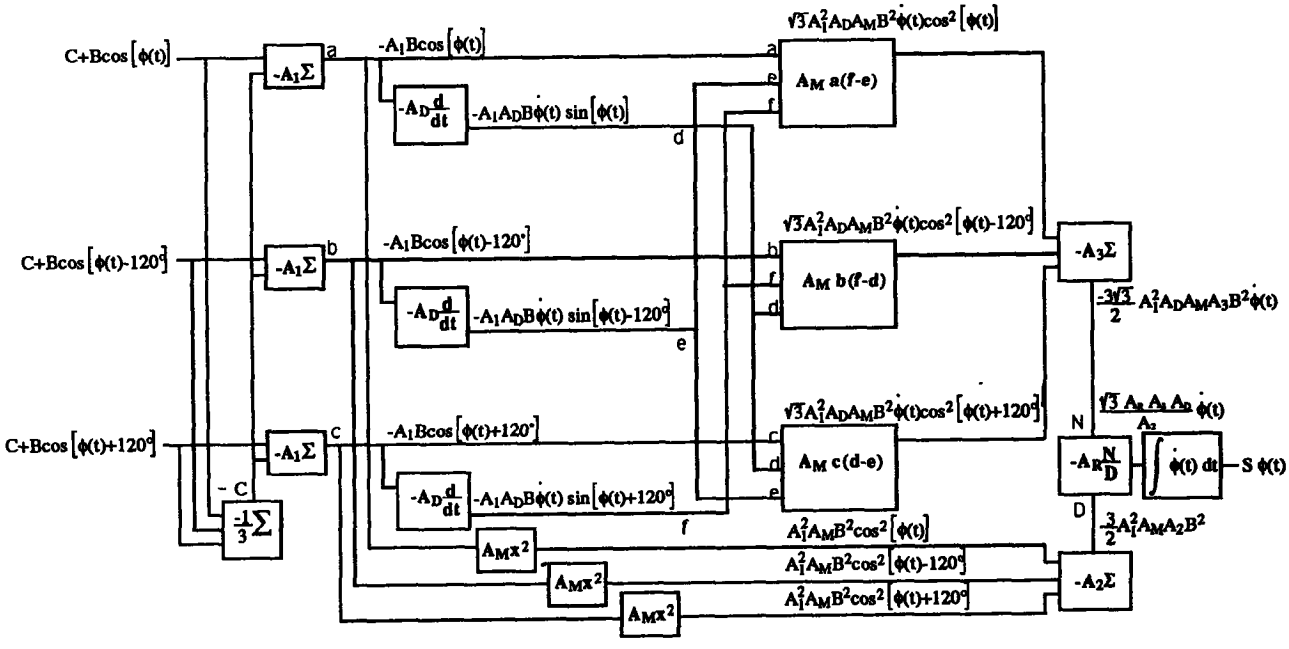

Figure 6. Block diagram of the passive symmetric interferometric signal demodulator signal flow using the outputs of a 3x3 optical fiber coupler. The outputs from each of the fibers are C + Bcos[ϕ(t)] and C + Bcos[ϕ(t) + 120°]. The stimuli-induced modulating signal, ϕ(t), is re-created at the output and is multiplied by scale factor, S.

The dynamic range of the demodulator is defined as the ratio of the maximum signal that can be accurately reproduced by the circuit to the minimum detectable signal in a given bandwidth. A conservative criteria defining the maximum signal was chosen as that amplitude for which the demodulated output produced a total harmonic distortion level (THD) of 4%. For the detectability, the bandwidth of the measurement has been normalized to 1 Hertz. The minimum detectable signal at 600 Hz is 220 μrad/√Hz and the 4% THD signal level is 140 radians, thus the dynamic range for this initial implementation is 116 dB [28], [29].

In evaluating the demodulator performance, the maximum and minimum signal levels were proportional to "1/f" (-20 dB/decade). For the maximum signal, this limit was due to the maximum fringe rate of the demodulator (65 krad/sec). The 1/f dependance in the minimum detectability was due to integration of the multiplier noise. This performance leads to a frequency independent dynamic range for the system, which is well suited for practical use, since laser noise, ocean noise, and many other systems exhibit noise power spectral densities which increases with decreasing frequency at low frequencies.

ACKNOWLEDGEMENTS

This work was supported by the Naval Postgraduate School Direct Funded Research Program, the National Oceanic and Atmospheric Administration, and the Naval Sea Systems Command.

REFERENCES

1. L. M. Lyamshev and Yu. Yu. Smirnov, "Fiber-optic sensors (review)," Akust. Zh. **29**, 289-308 (May-June, 1982).
2. T. G. Giallorenzi, J. A. Bucaro, A. Dandridge, G. H. Siegel, Jr., J. H. Cole, S. C. Rashleigh, and R. G. Priest, "Optical fiber sensor technology," IEEE J. Quantum Electron. **QE-18**(4), 626-665 (1982)
3. V. I. Busurin, A. S. Semenov, and N. P. Udalov, "Optical and fiber-optic sensors (review)," Kvantovaya Elektron. (Moscow) **12**, 901-944 (May 1985).
4. Thomas J. Hofler and Steven L. Garrett, "Thermal noise in a fiber optic sensor," J. Acoust. Soc. Am. **84** (2), 471-475 August 1988.
5. D. A. Brown, T. Hofler, and S. L. Garrett, " High snsitivity, fiber-optic, flexural disk hydrophone with reduced acceleration response," Fiber and Integrated Optics **8**(3), 169-191 (1989)
6. C. M. Crooker and S. L. Garrett, "Fringe rate demodulator for fiber optic interferometric sensors," in *Fiber Optic and Laser Sensors V*, Proc. Soc. Photo-Optical Inst. Eng. (SPIE) **838**, 329 (1987)
7. E. F. Carome, "Acousto-optic transduction in optical fibers and in fiber optic acoustic devices," in *Frontiers in Physical Acoustics*, edited by D. Sette (Soc. Italiana di Fisica, Bologna, 1986), pp. 476-505.
8. S. L. Garrett and D. L. Gardner, Multiple axis fiber optic interferometric seismic sensor, U. S. Patent No. 4,893,930, Jan. 16, 1990.
9. D. L. Gardner and S. L. Garrett, "Fiber optic seismic sensor," in *Fiber Optic and Laser Sensors V*, Proc. Soc. Photo-Optical Inst. Eng. (SPIE) **838**, 271 (1987)
10. A fiber-optic interferometric seismic sensor with hydrophone applications, LCDR D. L. Gardner, Doctor of Philosophy in Engineering Acoustics, September 1987. NTIS Report No. AD B112-487
11. D. A. Brown and S. L. Garrett, "An interferometric fiber optic accelerometer", in *Fiber Optic and Laser Sensors VIII*, Proc. Soc. Photo-optical Inst. Eng. (SPIE), **1367**, 282-288, (1990).
12. D. A. Brown, T. Hofler , and S. L. Garrett, Flex disc accelerometer, Patent application, Navy case 73054 (1991).
13. D. L. Gardner and S. L. Garrett, "High-sensitivity fiber-optic compact bidirectional hydrophone (U)," CONFIDENTIAL, U.S. Navy J. Underwater Acoust. JUA(USN) **38**(1), 1-21 (January, 1988)
14. D. L. Gardner, R. K. Yarber, E. F. Carome, and S. L. Garrett, "Fiber-optic interferometric geophone with hydrophone applications," 6th Int. Conf. on Integrated Optics and Optical Fiber Communications (Jan. 1987)
15. D. A. Brown, T. Hofler, and S. L. Garrett, "High-sensitivity, fiber-optic, flexural disk hydrophone with reduced acceleration response", Fiber and Intergrated Opt. **8**, 169-191 (1989).
16. D. A. Brown, T. Hofler, and S. L. Garrett, "A fiber-optic flexural disk microphone", in *Fiber Optic and Laser Sensors VIII*, Proc. Soc. Photo-optical Inst. Eng. (SPIE), **985**, 172-182, (1988).
17. T. Hofler and S. L. Garrett, Flexural disk fiber optic interferometric omnidirectional hydrophone, U. S. Patent No. 4,959,539, September 25, 1990.

18. S. L. Garrett, D. A. Brown, B. L. Beaton, K. Wetterskog, and J. Serocki, "A general purpose fiber-optic hydrophone made of castable epoxy", in *Fiber Optic and Laser Sensors VIII*, Proc. Soc. Photo-optical Inst. Eng. (SPIE), **1367**, 13-29, (1990).
19. S. L. Garrett and D. A. Danielson, Fiber optic interferometric ellipsoidal flextensional hydrophone, U. S. Patent No. 4,951,271, August 21, 1990.
20. D. A. Danielson and S. L. Garrett, "Fiber-optic ellipsoidal flextensional hydrophones", J. Lightwave Tech. 7(12), 1995-2002 (1989).
21. Optical fiber interferometric acoustic sensors using ellipsoidal shell transducers, D. A. Brown, Doctor of Philosophy in Engineering Acoustics, June 1991
22. S. L. Garrett and D. A. Brown, "Fiber-optic push-pull hydrophones", DoD Conference on Fiber Optics, McLean, VA, March, (1990).
23. A. Dandridge, A. B. Tveten, T. G. Giallorenzi, "Homodyne demodulation scheme for fiber optic sensors using phase generated carrier," IEEE Journal of Quantum Electronics, QE-18(10), October 1982.
24. A. Dandridge and A. B. Tveten, "Phase compensation in interferometric fiber-optic sensors," Optics Letters, 7(6), June 1982
25. C. B. Cameron, "Recovering Signals from Optical Fiber Interferometric Sensors", Ph. D. Dissertation, Electrical Engineering, Naval Postgraduate School, Monterey, CA, June, 1991.
26. S. K. Sheem, "Optical fiber interferometers with [3x3] directional couplers: Analysis," J. Appl. Phys. **52**, 960, June 1981.
27. K. P. Koo, A. B. Tveten, and A. Dandridge, "Passive stabilization scheme for fiber interferometers using (3x3) fiber directional couplers," Appl. Phys. Lett. **41**(7), October 1982.
28. M. A. Davis, A. D. Kersey, M. J. Marrone, and A. Dandridge, "Chartacterization of 3x3 fiber couplers for passive homodyne systems: Polarization and Temperature Sensitivity," paper WQ2, *Proc. Optical Fiber Communications Conference*, Houston, TX, Feb. 6-9, 1989.
29. C. B. Cameron, R. M. Keolian, and S. L. Garrett, "A Symmetric Analogue Demodulator for Optical Fiber Interferometric Sensors", Proc. 34th Midwest Symposium on Circuits and Systems (IEEE), Monterey, CA, May 14-17, 1991.